Spatiotemporal Sedimentary Facies Variations in the Lower Permian Whitehill Formation, Ecca Group, Karoo Basin

10

Kenneth Chukwuma and Emese M. Bordy

Abstract

The Lower Permian Whitehill Formation in the Karoo Basin is a potential shale gas unit in South Africa. Recharacterizing this heterogeneous formation and explaining the spatiotemporal variations in its geometry, texture, bedding features, composition, and distribution of organic carbon content is necessary, because gas recovery can be strongly influenced by these characteristics of the host rock. Here, we report on these rock property variations and their sedimentological controls in light of recent advances in shale sedimentology by combining field descriptions, petrographic observations and geochemical proxies. We distinguish five sedimentary facies (F1–F5) that suggest changes in the Early Permian depositional conditions from overall low energy in F1 and F2, allowing pelagic snow aggregates to cover the basin floor, to higher energy in F3, F4, and F5, bringing terrestrial detritus via hyperpycnal and diluted mud flows, which possibly originated from summer melting of mountain glaciers in the Cargonian Highlands flanking the northern margin of the Karoo Basin.

Keywords

Karoo basin • Shale gas • Permian • Mud depositional setting • Sedimentary facies

10.1 Introduction

The Lower Permian Whitehill Formation (WHF) has attracted attention from geologists for over a century (e.g., Rogers and Du Toit 1909; Schwarz 1912; Cunningham-Craig 1914) due to the oil shale potential, abundant but low diversity fossil biota and conspicuous white-weathering characteristics of this black, carbonaceous shale unit. Currently, renewed interest in the WHF is due to its perceived shale gas potential (e.g., Decker and Marot 2012; Geel et al. 2013, 2015; Smithard et al. 2015). However, despite a large number of publications on its lithology (e.g., Cole and McLachlan 1991; Visser 1992), sedimentology (e.g., Visser 1992), paleontology (e.g., Oelofsen 1981, 1987) and hydrocarbon potential (e.g., Rowsell and de Swardt 1976; Cole and McLachlan 1991; Geel et al. 2013; Smithard et al. 2015), the WHF remains poorly understood. For instance, while reference is often made to this black, thinly laminated, carbonaceous formation as a typical anoxic facies, no consensus exists on the palaeo-water depths (e.g., Oelofsen 1981, p. 21, 143; Cole and McLachlan 1991, p. 381) or salinity levels (e.g., Faure and Cole 1999 vs. Scheffler et al. 2006). Furthermore, the widely accepted anoxic facies model requires refinement to explain why the WHF contains more siltstone and very fine-grained sandstone than 'black shale' in the northeastern part of the Karoo Basin (e.g., Cole and McLachlan 1991; Werner 2006). Its regional geometry (e.g., thinning from SW to NE) and style of mud sedimentation (e.g., Visser 1992; Werner 2006) also need additional research. The distribution of organic carbon in the formation is uneven both laterally across the basin and vertically within stratigraphic sections (Cole and McLachlan 1991; Geel et al.

K. Chukwuma · E.M. Bordy (✉)
Department of Geological Sciences, University of Cape Town, Cape Town, 7701, South Africa
e-mail: emese.bordy@uct.ac.za

K. Chukwuma
e-mail: chkken003@myuct.ac.za

B. Linol and M.J. de Wit (eds.), *Origin and Evolution of the Cape Mountains and Karoo Basin*,
Regional Geology Reviews, DOI 10.1007/978-3-319-40859-0_10

2013; Smithard et al. 2015). While some areas are enriched in total organic carbon (up to 17 % TOC; Cole and McLachlan 1991), others are organic carbon-lean with less than 1 % TOC. Quantifying the interplay of syn- vs. post-depositional controls (e.g., structural deformation and metamorphism) on the TOC distribution in the WHF on a basinal scale is lacking, with the exception of a few localities that were studied in recent publications (e.g., Geel et al. 2013; Smithard et al. 2015, see also Chaps. 7 and 8 in this book).

Recently, significant hydrocarbon reserves have been associated with 'black shales' globally. This, together with developments in horizontal drilling and multistage fracture stimulation technology have triggered an unprecedented interest in the sedimentology and stratigraphy of these 'black shales' worldwide (e.g., Bohacs et al. 2005; Macquaker et al. 2010; Lazar et al. 2015; Wilson and Schieber 2015), and nationally in the WHF, the singular rock unit with ambient qualities for shale gas exploitation in South Africa. This study aims to: document the variations in the internal composition and primary sedimentary features of the WHF, and to analyze the link between the facies changes and the dynamics of sedimentation in time and space.

10.2 Geological Background

The WHF is part of the Permian Ecca Group, which in turns is part of the Upper Carboniferous to Lower Jurassic Karoo Supergroup. With an estimated thickness ranging between 30 to no more than 100 m, the WHF forms an outcrop belt along the western and southern portion of the Karoo Basin. It has been identified in the subsurface, where it ranges in depth from 1600 to 3000 m below surface, and thus the formation occupies an area of $\sim$235,000 km^2 in the western half of the basin (inset Fig. 10.1; Visser 1992; Tankard et al. 2012). Stratigraphically, the WHF occurs between the Prince Albert and Collingham Formations in the south and between the Prince Albert and Tierberg Formations in the west. It is correlated with the upper part of coal-bearing Vryheid Formation in the northeastern part of the basin (Cole and McLachlan 1991; Visser 1992). Based on palynology, litho- and bio stratigraphy, the WHF is also correlated with the Irati Formation in the Paraná Basin of southeastern Brazil (Oelofsen 1987; Chap. 18 in this book). In spite its tuffaceous beds, radiometric dates are not available for the WHF in South Africa. Absolute dates from the WHF correlative units are 280.5 $\pm$ 2.1 Ma in Namibia (Werner 2006) and 278.4 $\pm$ 2.2 Ma in Brazil (Santos et al. 2006), and therefore the WHF in South Africa is inferred to be Kungurian in age.

At outcrop-scale, the white-weathering formation is distinguished from the dark to olive gray lithologies of the under- and overlying Prince Albert and Collingham/Tierberg Formations. When freshly exposed, the WHF is predominantly black (Fig. 10.2), thinly laminated shale with vertical and lateral variations in silt content (Oelofsen 1981, 1987; Cole and McLachlan 1991; Visser 1992). Nodules of carbonate, pyrite and chert, evaporites (e.g., gypsum, halite), as well as pale gray to yellowish thin tuffaceous beds are also present (e.g., McLachlan and Anderson 1977, 1979; Oelofsen 1981, 1987; Cole and McLachlan 1991; Visser 1992; Faure and Cole 1999; Werner 2006). Visser (1992) subdivided the WHF into SW deep- and NE shallow-water facies mainly based on the distribution of post-depositional, diagenetic sedimentary features (e.g., chert) and not on the primary characteristics of the sedimentary facies such as lithology, texture, suite of sedimentary structures, geometry, fossils (e.g., Tucker 2011).

The lower part of the WHF is largely unfossiliferous, whereas the upper half hosts a highly diverse fossil assemblage comprising aquatic mesosaurid reptiles, palaeoniscid fish, crustaceans, insects, as well as terrestrial plant debris (e.g., palynomorphs, gymnosperms wood, *Glossopteris* sp. leaves, club mosses—McLachlan and Anderson 1973, 1977; Oelofsen 1981; Cole and McLachlan 1991). Ichnofossils, in addition to unidentified bioturbation, include arthropod tracks, fish swimming traces and coprolites (Oelofsen 1981, 1987). The stratigraphic distribution of the fossils as well as carbon and pyrite prompted McLachlan and Anderson (1977) and Oelofsen (1981, 1987) to argue for a stratified Early Permian water body in the Karoo Basin (see also Chap. 11 in this book), where the anoxic reducing bottom conditions contrasted the oxygenated surface conditions that supported free swimming, benthic and platonic organisms. Paleontological evidence for a marine affinity of the WHF fossils is lacking (e.g., McLachlan and Anderson 1973, 1979; Faure and Cole 1999).

10.3 Methods

WHF outcrops were studied to capture the facies heterogeneity, which can be detected in the texture, fabric and bedding features as well as composition. The exposed WHF strata were logged sedimentologically, photographed, and sampled along the entire outcrop belt, except in the easternmost part of the Eastern Cape where the WHF is very poorly exposed (Fig. 10.1). The microtexture, mineralogy of the matrix fraction and cement were established using standard petrographic investigations and Carl Zeiss MERLIN and EVO high resolution field emission scanning electron microscope (FE-SEM) with nanoscale and micro- and cryo-EDS operated mainly in back scatter and cathode luminescence modes between 20 and 30 kV at 9–11 mm working distance. Total organic carbon content was measured with LECO CS244 carbon analyzer at the Indian Institute of Technology in Bombay.

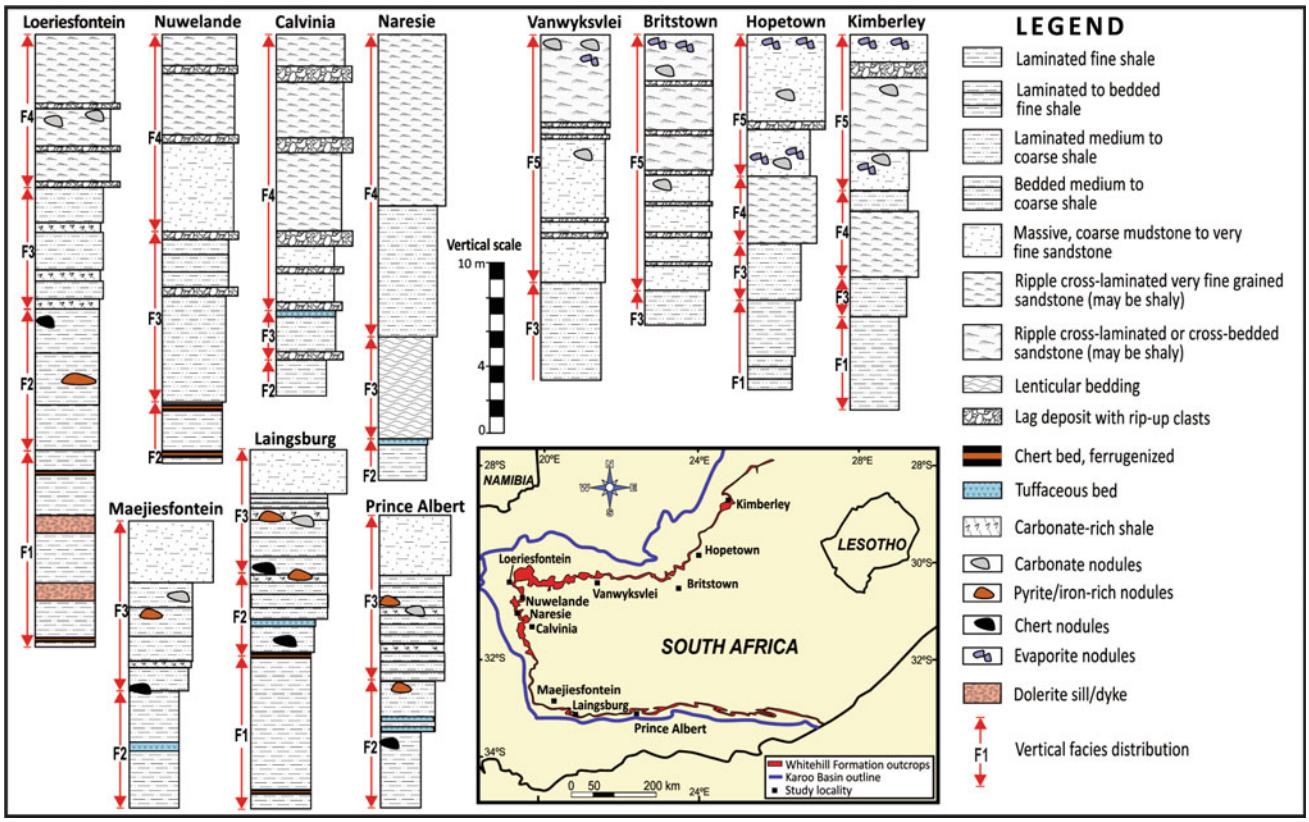

Fig. 10.1 Simplified sedimentological logs of the WHF measured in selected outcrops in the western Karoo Basin. Thicknesses reported are not the maximum thickness of the formation at those localities, but the maximum exposed thickness of the facies at each locality. The base of F1 and top of F5 when exposed are either sharp or gradational. For log locations refer to the inset map which also shows the areal distribution of the WHF outcrops in the basin. Note that F4 and F5 are only found along the northern margin of the WHF outcrop area

10.4 Observations

Five distinctive facies (F1–F5) of the WHF can be recognized (Table 10.1) that include fine- to coarse-grained shales (*sensu* Lazar et al. 2015) with a variety of primary sedimentary features, which are mainly fine laminations, very thin and thin (1–5 cm) beds in F1 and F2 that give way to an upward increasing abundance horizontal- to low-angle cross-laminations, internal scours, sharp bedding planes, diffuse bedding, as well as, normal graded beds (from coarse silt to clay) in F3, F4 and F5 (Fig. 10.4, Table 10.1). Ripple cross-laminations with forest dip directions ranging between 44° and 78° (E–NE) were measured in F4 and F5 between Calvinia and Loeriesfontein (Figs. 10.1 and 10.4). Body fossils of mesosaurid reptiles, palaeoniscoid fish, plant fragments, fish trails were observed in F3, F4 and F5 between Calvinia and Vanwyksvlei (Figs. 10.1 and 10.2). The southern KB outcrops only yielded some poorly preserved plant fragments in F3 (e.g., east of Prince Albert; Fig. 10.2). In contrast the facies contain variable quantities of organic carbon that ranges from 0.1 to 16.5 wt% in F5 and F2, respectively. Dark colored chert and carbonate concretions (up to 3 m in diameter) and beds (up to 1.4 m) are common in the lower part of the formation, particularly in F2, and light gray to yellowish carbonate and evaporite concretions are mainly present in F4 and F5. Yellowish-weathering thin tuffaceous beds occur throughout the formation (e.g., an 8 cm layer was recorded in F3 near Calvinia; Fig. 10.1). Primary fabrics are occasionally overprinted by secondary alteration features (e.g., mineral filled cracks). In the Tankwa area, the shales are gently deformed and dip southward between 2° and 6°, whereas between Calvinia and Loeriesfontein the dip is 2°–3° northward. Between Vanwyksvlei and Hopetown, the shales dip southward at 2° and 7°. In contrast to the northern study sites, bed thickness and orientation are harder to define in the south due to structural deformation associated with the Cape orogeny (Fig. 10.1).

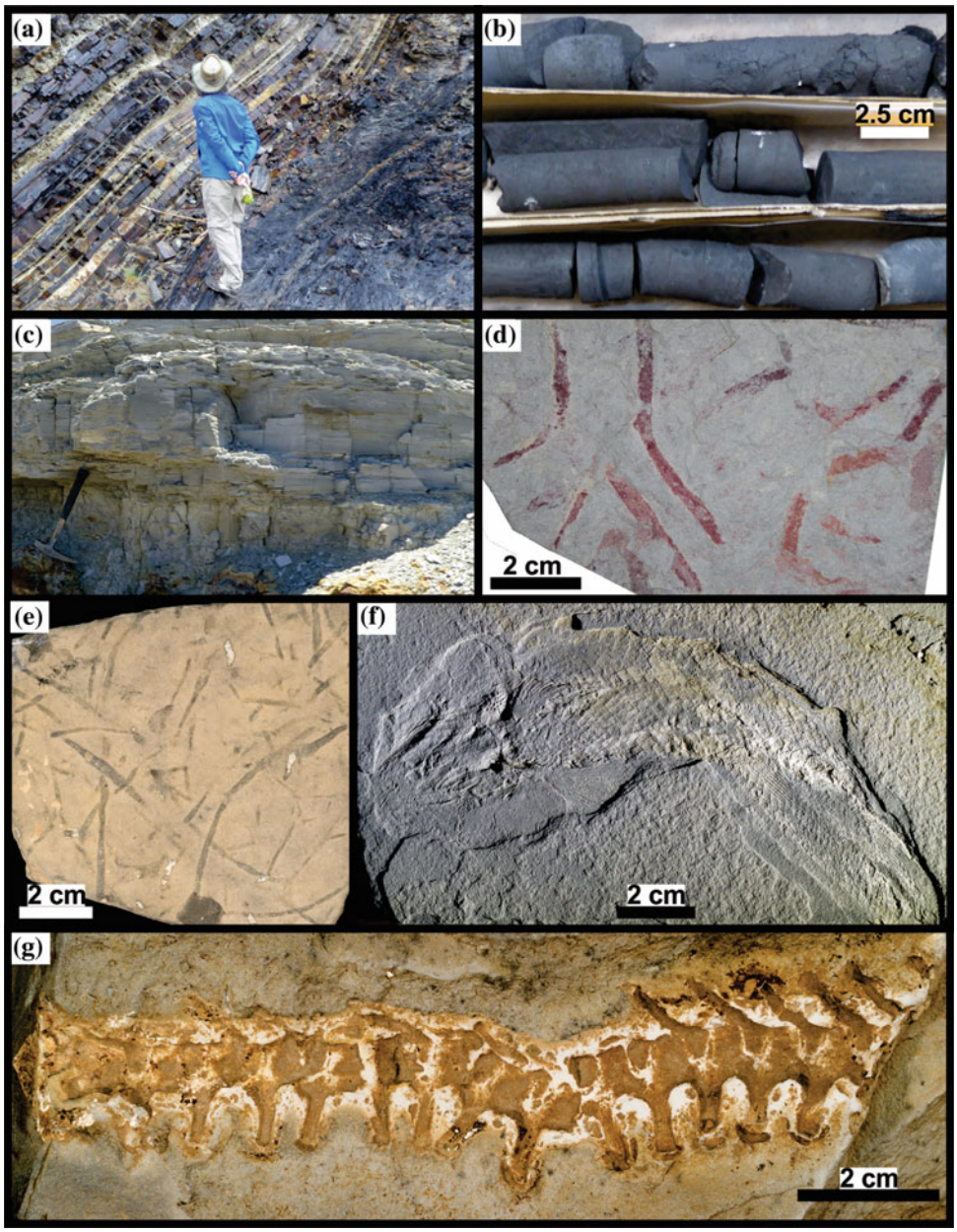

Fig. 10.2 **a** Outcrop image of the crisp contact between Whitehill and Collingham Formations (on the *right* and *left*, respectively) near Laingsburg. **b** Freshly drilled outcrop samples obtained with a portable hand drill fitted with a 400 × 25 mm drill barrel. Core diameter is 2.5 cm. **c** Sharp-based and normally graded light gray to white shales and very fine-grained sandstones are common in the northern outcrop area (F5). Hammer is 31.3 cm long. **d** Plant fragments in middle WHF (near Prince Albert; F3). **e** Trace fossil are common in the in middle WHF (near Nuwelande; F3). **f** Body fossil of palaeoniscid fish found in F4 near Nuwelande. **g** Body fossil of mesosaurid reptile (dorsal spine) found in F4 near of Calvinia. Mesosaurids were endemic to SW Gondwana in the Early Permian

10.5 Discussion

10.5.1 Depositional Processes

Dominance of biogenic detritus, thin laminations and close association between clay fraction and organic matter (OM—e.g., flattened algal macerals; Fig. 10.2) packaged as organo-minerallic aggregates ('org-min-a') in F1 and F2 indicate that these sediments were: (1) produced in an overall low energy water body away from the reach of coarse clastic sedimentary detritus and (2) settled out of buoyant suspensions in form of pelagic snow aggregates (e.g., Fowler and Knauer 1986; Bohacs et al. 2005; Macquaker et al. 2010). Mud-size particles do not only settle out of suspension individually, but often clump together due to physical coagulation and/or zooplankton-mediated aggregation (e.g., Nittrouer et al. 1986; Alldredge and Gotschalk 1990). In the latter, the organo-minerallic aggregates are glued together by extra-cellular muco-polysaccharides and exopolymeric secretions of plankton (e.g., Fowler and Knauer 1986; Faure and Cole 1999).

The disseminated fine-grained (<5 μm) pyrite framboids in F1 (Fig. 10.2) suggests that this facies may have been deposited on the basin floor where sulfidic and anoxic conditions existed (Demaison and Moore 1980; Wignall and Newton 1998; Lazar et al. 2015). In contrast, pyrite grains aligning

Table 10.1 Summary of the sedimentary facies in the Whitehill Formation (also see Figs. 10.1, 10.2, 10.3 and 10.4). Fossils content is based on observations in this study and reports in Oelofsen (1981)

Facies code	Facies description	Sedimentary process interpretation
F1	Thinly and horizontally laminated (~5 mm-thick), black, carbonaceous, fine shale with an average TOC of 4.4–7.8 wt%; contains flattened organo-minerallic aggregates (oma), amorphous organic carbon, fecal pellet-like materials, disseminated fine-grained (<5 μm) pyrite framboids/concretions, and minor silt-size quartz with some pyrite-filled hair cracks; few grains of barite; the matrix is clay (illite-smectite), amorphous organic carbon (aoc), chert/quartz. No fossils found or reported to date	High bioproductivity; suspension settling of pelagic snow on the basin floor at the anoxic and sulfidic water–sediment interface
F2	Laminated to bedded, black, splintery argillaceous fine shale with a maximum TOC of ~16.5 wt%; Contains silt-size quartz, clay, aoc, fecal pellets, algal maceral and pyrite majorly aligned along bedding planes; Few mm to 10 m diameter diagenetic nodules common in upper section; the matrix is clay, carbonate, aoc, quartz. No fossils found or reported to date	Suspension settling of pelagic snow under intermittent anoxic and sulfidic iron-poor sediment-water conditions. Initial high bioproductivity was interrupted, resulted in early cementation and remineralization
F3	Sharp-based, horizontally laminated to bedded occasionally burrowed, diminutive normally graded, dark gray siliceous-calcareous-argillaceous medium shale; Contains silt-size quartz, clay, aoc, fecal pellets and lags of rip-up shale particles, with an average TOC of 1.6 wt%; the matrix is clay, quartz, carbonate. Trace fossils are common (include: fish swimming traces, arthropod tracks, horizontal and interconnecting burrows); fragmentary plant fossil east of Prince Albert	Erosion and redeposition of muddy substrate by currents in sustained bed-load transport; incipient oxic bottom waters
F4	Horizontal and ripple cross-lamination, diffused bedding, internal scouring, gray siliceous medium shale with continuous nonparallel down-lapping (concave-up) geometries and triplet features; average TOC: 1.01 wt%; the matrix is quartz, carbonate ≫ clay. Mesosaurid reptiles and palaeoniscoid fish are abundant in the lower part of F4	Progressive dominance of waning wave-enhanced sediment gravity flows and bed-load dominated currents; often transient oxic bottom waters, especially in the upper part of F4
F5	Horizontal and ripple cross-lamination to massive, diffused bedding, light gray siliceous coarse-grained shale with continuous nonparallel down-lapping (concave-up) geometries and triplet features; thicker beds than in F4; average TOC: 0.58 wt%; the matrix is quartz and carbonate. Palaeoniscoid fish, and in the upper part, pygocephalomorphic crustaceans (e.g., *Notocaris tapscotti*) are abundant	Rapid, *en masse* deposition of sand and silt in hyperpycnal flows and bed-load dominated currents; often fully oxygenated water body

bedding planes of F2 indicate presence of free oxygen at the sediment–water interface (e.g., Lazar et al. 2015). The intergranular pores-filling clays and quartz in F1 and F2 (Fig. 10.2) indicate their diagenetic origin (e.g., Macquaker et al. 2014; Lazar et al. 2015). The diagenetic nodules with well-developed carbonate cement, and pre-compaction microcrystalline pyrite cement in F2 (Fig. 10.2) further attests that the pore water contained microbial reduced sulfate whose solutes filled the pores prior to compaction and initiated the growth of nodules, following a pause in sedimentation(e.g., Dean and McArthur 1989; Macquaker and Gawthorpe 1993). Furthermore, the change from thin lamination of F1 to alternation of laminated and non-laminated beds in F2 (Figs. 10.1 and 10.3) suggest disruption to the anoxia during F1.

The marked increase in the quantity of coarse-grained silt and very fine-grained sand particles from F3 to F5, together with an upward increasing abundance of horizontal- to cross-laminations, internal scours, sharp bedding planes, diffuse bedding, as well as, normal graded beds (Figs. 10.1, 10.2, 10.3 and 10.4; Table 10.1) are interpreted as products of sustained lateral sediment transport by turbulent flows with waxing and waning current energies (Macquaker et al. 2010; Wilson and Schieber 2015). The increasingly higher energy levels during deposition of F3–F5 are also attested by several shale layers with subrounded to subangular rip-up particles with diameters up to 1.1 mm (Fig. 10.1). These intraformational shale particles (Fig. 10.3g, h) may also be used as an indirect evidence for the above postulated pause

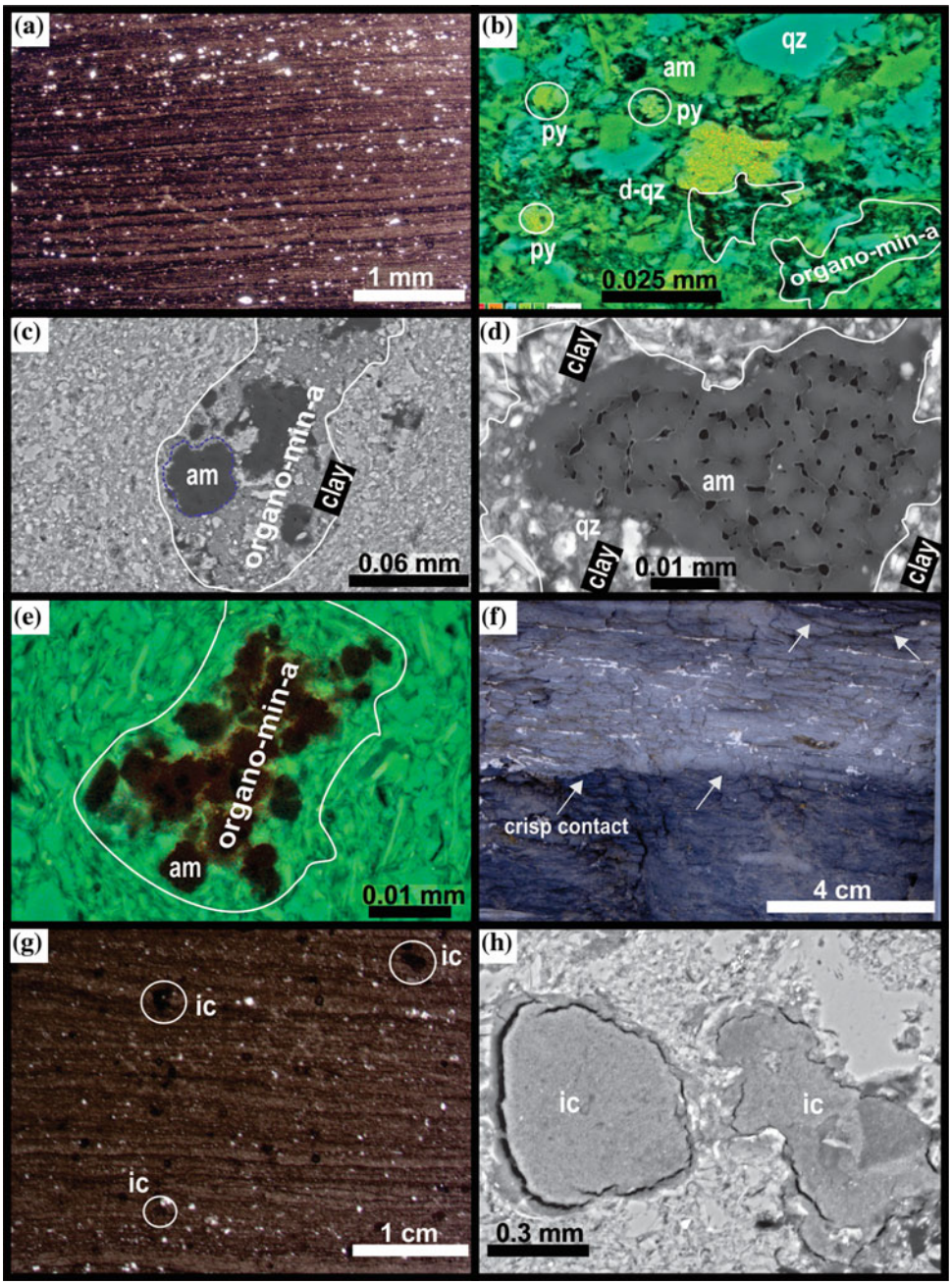

Fig. 10.3 Micro-sedimentary features (structure, fabric, texture) of F1, F2 and F3 in the WHF. **F1 a** Optical photomicrograph of uniform, continuous horizontal laminations. **b** Back-scattered electron photomicrograph of disseminated pyrite (py) and the association of algal macerals (am), pellets, and clay that form organo-minerallic aggregates (org-min-a—*white outlines*). Diagenetic quartz (d-qz) infills intergranular pores. Organic carbon, pre-compaction microcrystalline carbonate and pyrite cement indicate that pore waters controlled microbial reduction. The sulfate, likely derived from the water column, infilled the sediment pores pre-compaction and/or during a pause in sedimentation (e.g., Dean and McArthur 1989; Macquaker and Gawthorpe 1993). **F2 c** Back-scattered electron photomicrograph of close knitting between algal macerals and clays ('org-min-a'—*white outline*). **d** Close-up of features in the am shown in **c**. The 'org-min-a' are larger in F2 compared to F1. Pores are filled by quartz and clay. **e** Close-up of the algal macerals (am) and organo-minerallic aggregate (org-min-a—*white outlines*). **F3 f** Horizontally laminated to bedded, medium shales with crisp contacts (arrows). **g** Optical photomicrograph of intraclasts (ic) and vertical variability in lamina thickness. **h** Back-scattered electron photomicrograph of G showing the close-up of the subrounded to subangular intraclasts (ic), which are rip-up shale particles with diameters up to 1.1 mm

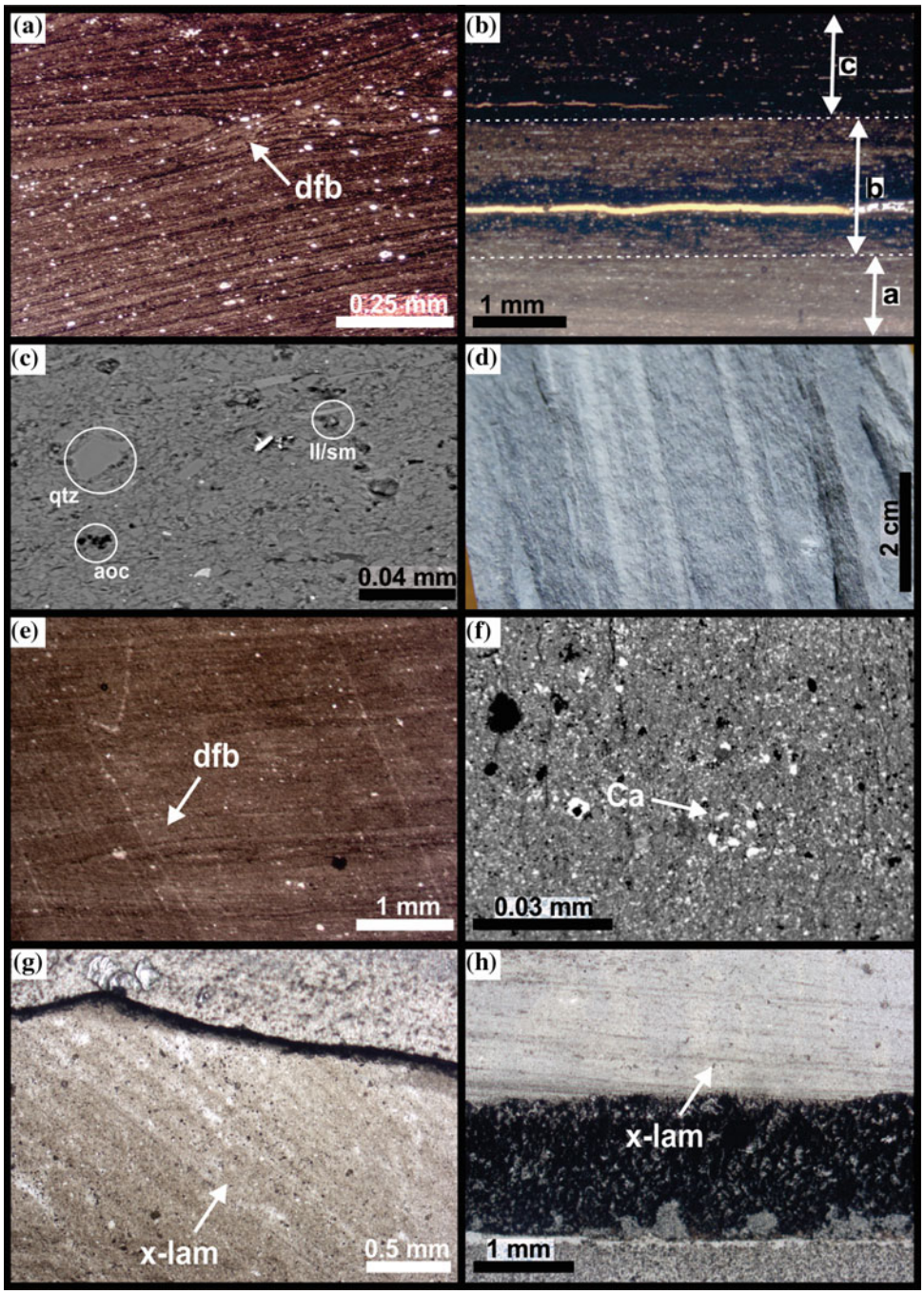

Fig. 10.4 Micro-sedimentary features (structure, fabric, texture) of F4 and F5 in the WHF. **F4 a** Optical photomicrographs of diffused bedding (dfb) and concave upward geometries. **b** Optical photomicrograph of triplet feature. Note the gradual increase in clay content (darker laminae). **c** Back-scattered electron photomicrograph illustrating the dominance of clay and quartz particles. **F5 d** Horizontal interlamination of clay- and silt-rich layers in a shale hand specimen. **e** Optical photomicrographs of diffused bedding (dfb) and concave upward geometries. **f** Back-scattered electron photomicrograph illustrating the grain size and mineral composition (mainly clay and quartz) in **c**. **g** Optical photomicrograph of ripple cross-lamination (x-lam). Note the steep dip angle of the foresets, truncated by an erosion surface. **h** Optical photomicrograph of low-angle ripple cross-lamination (x-lam) in tangential contact with the lower bedding plane

in sedimentation that might have contributed to the consolidation of the previously deposited mud (F1–F2). The medium to coarse shale beds with sharp bases, horizontal and ripple cross-laminations, diminutive normal grading, and diffused bedding in F3–F5 (Figs. 10.1, 10.2, 10.3 and 10.4; Table 10.1), coupled with the higher abundance of trace and body fossils, suggest increasing oxygenation levels and higher clastic/nutrient influx to the basin floor, which were significant changes in sedimentary conditions relative to those lower energy and more anoxic ones that dominated during F1–F2. These interpretations are also supported by the northeast–southwest aligned fossils in F4–F5 and very low amplitude oscillation ripple marks found by Oelofsen (1981, p. 24) near Hopetown, Loeriesfontein and Calvinia. These symmetrical ripple marks recovered by Oelofsen occur within a facies that could correspond to the transition

of F3 and F4. The overall facies descriptions and interpretations presented here are also in line with sedimentological results of Cole and McLachlan (1991).

10.5.2 Orientation of the Basinal Paleo-slope

Palaeoslope of the basin at the time of deposition of the WHF is difficult to establish, because of the monotony of finely laminated shales with palaeocurrent indicators limited to rare cross-laminations, ripple marks and orientation of fossils (i.e,. 47 mesosaurid and 138 pygocephalomorphic crustacean specimens reported in Oelofsen 1981; his Figs. 9 and 10). Sedimentological and taphonomic evidence suggest that the ripples and the northeast–southwest aligned fossils were generated by weak, localized oscillatory flows rather than strong, unidirectional, basinal bottom currents. These localized flow indictors are unsuitable to infer the Early Permian basinal palaeoslope orientation (cf. Tucker 2011). Notwithstanding the lack of reliable primary palaeocurrent indicators in the WHF, the basinal distribution of the F3–F5 (Fig. 10.1) may be linked to a south-southwestward dipping WHF palaeoslope.

10.5.3 Depositional Setting Interpretations

Our results are in line with previous interpretations that suggest stratified and brackish water body across southwest Gondwana during the Kungurian (e.g., McLachlan and Anderson 1973; Faure and Cole 1999; Werner 2006; Flint et al. 2011). During the deposition of facies that are unfossiliferous and have high organic carbon content (F1 and F2), we interpret that the surface waters contained nutrients (e.g., N, Si, P, Fe) that enabled high primary productivity of OM, which was preserved together with fine-grained sediments on the basin floor under reducing (oxygen-depleted) conditions. Sediment-laden underflows subsequently entered the basin along its northern margin, possibly from summer melting of mountain glaciers north of the Karoo Basin (Cargonian Highland; see also Chap. 9 in this book). Consequently, the biogenic constituents produced were diluted by progressively higher input of terrestrial detritus. The contrast between the brackish and freshwater fluids possibly triggered thermohaline currents as the hyperpycnal riverine discharge plunged into the basin floor, eroding and resuspending the muddy substrate. Considering the basinal extent of F3 (Fig. 10.1), bottom hugging currents (diluted mud flows) probably moved the sediment over large distances on relatively low gradient slopes (<0.7°—e.g., Mulder et al. 2003; Bhattacharya and MacEachern 2009). Similar processes and features were observed on modern muddy shelves near river mouths (Friedrichs and Wright 2004), for example, at the mouths of the Yellow (Wright et al. 2001) and Amazon Rivers (Kineke et al. 1996), along the northern California coast (Eel River; Nittrouer et al. 1986; Wright et al. 2001), and in laboratory experiments (e.g., Schieber and Yawar 2009). Our depositional model (Fig. 10.5), which proposes an overall shallowing upwards trend and basinward migration of the shoreline along the southward dipping WHF palaeoslope, is supported by: (1) up-section increase in grain size, thickness, sharp bedding planes, graded intervals, layers with rip-up shale particles; (2) the spatiotemporal distribution of the facies—i.e., the basinal extent of F1–F3 versus the restricted nature of F4 and F5 along the northern margin of the basin (Fig. 10.1); and (3) reduced TOC in F4 and F5.

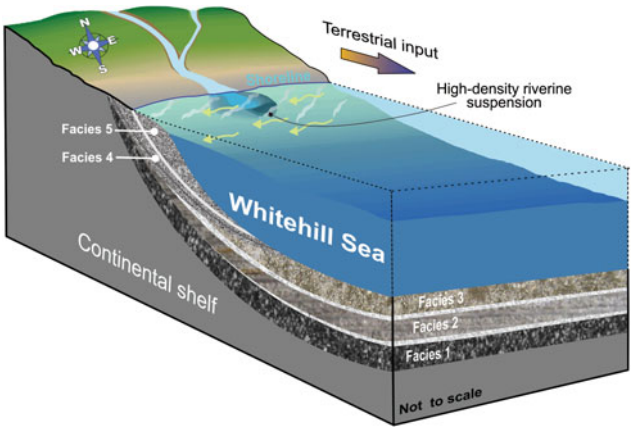

Fig. 10.5 Summary of the depositional model for the WHF showing spatial distribution of the five facies (F1–F5) deposited by diverse sedimentary processes. The near-uniform and basinal extent as well as predominant fine-grained size of F1 and F2 point to a low energy shelfal setting, away from coarse clastic inputs, in the distal parts of a large water body. Increase in grain size and detrital fractions in F3–F5 indicate progradation in a regressing water body. Compositional and textural differences of the facies (Figs. 10.1, 10.2, 10.3 and 10.4; Table 10.1) attest to variable provenance and complex sediment dispersal histories

10.6 Conclusion

Five distinctive facies in WHF reveal that in addition to the quiet settling of suspended particles, more energetic depositional processes were also present in the Karoo Basin during the Early Permian. The WHF facies and their basinal distribution are linked to: (1) primary sediment production within the basin, (2) terrestrial clastic input from the Cargonian Highlands in the north to the basin, and (3) post-depositional alterations. F1 and F2 are interpreted as biologically produced pelagic snow aggregates that were deposited on the basin floor, remote from coarse sediment sources and under anoxic to dysoxic conditions, favorable to preservation of organic carbon, especially in the lower part

of F2. Terrestrial detritus is increasingly more dominant from F3 to F5, and this upward increase in clastic grains is interpreted to be linked to underflows from summer melting of mountain glaciers north of the Karoo Basin that fed the sediment-laden hyperpycnal currents along the northern margin of the basin and mud flows further to south. In summary, the temporal and spatial variations in the internal composition, primary sedimentary structures and distribution of organic matter in the WHF reflect the diversity of sedimentary conditions (e.g., sediment supply, energy levels, mode of transport) in time and space within the Early Permian Karoo Basin.

Acknowledgments We would like to give special thanks to our friends and colleagues Francisco Paiva and Sanda Spelman for field assistance. We thank Nicholas Laidler for his invaluable lab assistance. We also gratefully acknowledge the very constructive reviews by Hans-Martin Schultz, Maarten de Wit and Bastien Linol. The financial support of the Faculty of Science at the University of Cape Town toward this research is hereby acknowledged. Opinions expressed and conclusions arrived at are those of the authors and are not necessarily to be attributed to the UCT.

References

Alldredge AL, Gotschalk CC (1990) The relative contribution of marine snow of different origins to biological processes in coastal waters. Cont Shelf Res 10:41–58

Bhattacharya JP, MacEachern JA (2009) Hyperpycnal rivers and prodeltaic shelves in the Cretaceous seaway of North America. J Sed Res 79:184–209

Bohacs KM, Grabowski GJ, Carroll AR, Mankiewicz PJ, Miskellgerhardt KJ, Schwalbach JR, Wegner MB, Simo JA (2005) Production, destruction, and dilution: the many paths to source-rock development. In Harris NB (ed) The deposition of organic carbon-rich sediments: SEPM Spec Pub 82, 61–101

Cole DI, McLachlan IR (1991) Oil potential of the Permian WHF Shale Formation in the main Karoo Basin, South Africa. In: Ulbrich H, Rocha-Campos AC (eds), Gondwana Seven Proceedings, pp 379–390

Cunningham-Craig EH 1914 Report on the petroleum prospects in the Union of South Africa. The Government Printing and Stationery Office, Pretoria, UG3, pp 28

Dean WE, McArthur MA (1989) Iron-sulfur-carbon relationships in organic-carbon-rich sequences: Cretaceous western seaway. Am J Sci 289:708–743

Decker J, Marot J (2012) Investigation of hydraulic fracturing in the Karoo of South Africa. Annexure A, Resource Assessment, Petroleum Agency SA. Available at: http://www.dmr.gov.za/publications/viewdownload/182/854.html

Demaison GJ, Moore GT (1980) Anoxic environments and oil source bed genesis. AAPG Bulletin 64:1179–1209

Faure K, Cole D (1999) Geochemical evidence for lacustrine microbial blooms in the vast Permian main Karoo, Parana, Falkland Islands and Huab basins of southwestern Gondwana. Palaeogeography, Palaeoclimatology, Palaeoecology 152:189–213

Flint SS, Hodgson D, Sprague AR, Brunt RL, Van der Marwe WC, Figueiredo J, Prélat A, Box D, Di Celma C, Kavanagh JP (2011) Depositional architecture and sequence stratigraphy of the Karoo basin floor to shelf succession, Laingsburg depocentre, South Africa. Mar Pet Geo 28:658–674

Fowler SW, Knauer GA (1986) Role of large particles in the transport of elements and organic compounds through the oceanic water column. Prog Oceanogr 16:147–194

Friedrichs CT, Wright LD (2004) Gravity-driven sediment transport on the continental shelf: implications for equilibrium profiles near river mouths. Coast Eng 51:795–811

Geel C, Schulz H-M, Booth P, de Wit M, Horsfield B (2013) Shale gas characteristics of Permian black shales in South Africa: results from recent drilling in the Ecca Group Eastern Cape. Energy Procedia 40:256–265

Geel C, de Wit M, Booth P, Schulz H-M, Horsfield B (2015) Palaeo-environment, diagenesis and characteristics of Permian black shales in the lower Karoo Supergroup flanking the Cape Fold Belt near Jansenville, Eastern Cape, South Africa: Implications for the shale gas potential of the Karoo Basin. SAJG 118:248–274

Kineke GC, Sternberg RW, Trowbridge JH, Geyser WR (1996) Fluidmud processes on the Amazon continental shelf. Cont Shelf Res 16:667–696

Lazar OR, Bohacs KM, Macquaker JHS, Schieber J, Demko TM (2015) Capturing key attributes of fine-grained sedimentary rocks in outcrops, cores, and thin sections: nomenclature and description guidelines. J Sed Res 85:230–246

Macquaker JHS, Gawthorpe RL (1993) Mudstone lithofacies in the Kimmeridge Clay Formation, Wessex Basin, Southern England: implications for the origin and controls of the distribution of mudstones. J Sediment Petrol 63:1129–1143

Macquaker, JHS, Keller MA, Davies SJ (2010) Algal blooms and "marine snow": mechanisms that enhance preservation of organic carbon in ancient fine-grained sediments. J Sed Res 80:934–942.

Macquaker, JHS,Taylor KG, Keller MA, Polya D (2014) Compositional controls on early diagenetic pathways in fine-grained sedimentary rocks: Implications for predicting unconventional reservoir attributes of mudstones. AAPG Bull 98:587–603

McLachlan IR, Anderson AM (1973) A review of the evidence for marine conditions in Southern Africa during Dwyka times. Palaeontol Afr 15:37–64.

McLachlan IR, Anderson AM (1977) Carbonates, "stromatolites" and tuffs in the lower Permian White Band Formation. SAJG 73:92–94

McLachlan IR, Anderson AM (1979) The oil-shale potential of the Early Permian White Band Formation in Southern Africa. Geol Soc S Afr Spec Publ 6:83–86

Mulder T, Syvitski JPM, Migeon S, Faugères, JC, Savoye B (2003) Marine hyperpycnal flows: initiation, behavior and related deposits: a review. Mar Pet Geo 20:861–882. doi:10.1016/j.marpetgeo.2003.01.003

Nittrouer CA, Curtin TB, DeMaster DJ (1986) Concentration and flux of suspended sediment on the Amazon continental shelf. Cont Shelf Res 6:151–174

Oelofsen BW (1981) An anatomical and systematic study of the Family Mesosauridae (Reptilia: *Proganosauria*) with special reference to its associated fauna and palaeoecological environment in the WHF Sea. Unpublished PhD thesis, University of Stellenbosch, South Africa, pp 259

Oelofsen BW (1987) The biostratigraphy and fossils of the Whitehill and Irati Shale Formations of the Karoo and Parana Basins. In: McKenzie GD (ed), Gondwana Six Proceedings, pp 131–138

Rogers, A. W, Du Toit, A. L (1909) An introduction to the Geology of Cape Colony. Longmans, Green and Co. New York, Bombay, pp 491

Rowsell DM, de Swardt AMJ (1976) Diagenesis in Cape and Karroo sediments, South Africa, and its bearing on their hydrocarbon potential. Trans Geol Soc S Africa 79:81–145

Santos RV, Souza PA, Souza de Alvarenga CJ, Dantas EL, Pimentel MM, Gouveia de Oliveira C, Medeiros de Araújo L (2006) Shrimp U–Pb zircon dating and palynology of bentonitic layers from the Permian Irati Formation, Paraná Basin, Brazil. Gondwana Res 9:456–463

Schieber J, Yawar Z (2009) A new twist on mud deposition: mud ripples in experiment and rock record. The Sed Record 7:4–8

Smithard T, Bordy EM, Reid D (2015) The effect of dolerite intrusions on the hydrocarbon potential of the lower Permian WHF Formation (Karoo Supergroup) in South Africa and southern Namibia: A preliminary study. SAJG 118:489–510

Scheffler K, Buehmann D, Schwark L (2006) Analysis of late Palaeozoic glacial to postglacial sedimentary successions in South Africa by geochemical proxies - Response to climate evolution and sedimentary environment. Palaeogeog palaeoclim palaeoecol 240: 184–203

Swartz EHL (1912) South African Geology. Blackie and Son Ltd, London, Glasgow, Bombay, pp 200

Tankard A, Welsink H, Aukes P, Neweighton R, Stettler E (2012) Geodynamic interpretation of the Cape and Karoo basins, South Africa. In: Roberts, D.G, Bally, A.W (Editors), Regional Geology and Tectonics: Phanerozoic Passive Margins, Cratonic Basins and Global Tectonic Maps. Elsevier, U.K, pp 869–945

Tucker ME (2011) Sedimentary rocks in the field; A practical guide. Blackwell, Oxford, pp 275

Visser JNJ (1992) Deposition of the Early to Late Permian Whitehill Formation during a sea-level highstand in a juvenile foreland basin. SAJG 95:181–193

Werner M (2006) The stratigraphy, sedimentology and age of the Late Palaeozoic Mesosaurus Inland Sea, SW-Gondwana: new implications from studies on sediments and altered pyroclastic layers of the Dwyka and Ecca Group (lower Karoo Supergroup) in southern Namibia. Unpublished PhD Thesis, University of Würzburg, Germany, pp 428

Wignall PB, Newton R (1998) Pyrite framboid diameter as a measure of oxygen deficiency in ancient mudrocks. Am J Sci 298:537–552

Wilson RD, Schieber J (2015) Sedimentary facies and depositional environment of the Middle Devonian Geneseo Formation of New York, USA. J Sed Res 85:1393–1415

Wright LD, Friedrichs CT, Kim SC, Scully ME (2001) Effects of ambient currents and waves on gravity-driven sediment transport on continental shelves. Mar Geol 175:25–45